Coastal Dynamics 2017
Paper No. 155

A NEW SHORELINE INSTABILITY MECHANISM RELATED TO HIGH-ANGLE WAVES

Albert Falqués[1], Nabil Kakeh[1] and Daniel Calvete[1]

Abstract

A new shoreline instability triggered by high-angle waves and leading to sand wave formation is investigated. In contrast with the well-known high angle wave instability, which involves both the surf and shoaling zones and develops at km-scale wavelengths, the present mechanism involves only the surf zone. The emerging morphology features up-current oriented bars coupled to a meandering of the longshore current. The dominant wavelengths scale with the surf zone width, X_b = O(10^2 m) and the characteristic growth times are O(1 day). The instability occurs only above a critical angle ~ 30^o in deep water and its maximum intensity is for ~ 70^o. It is associated to the gradients in longshore transport and, for wavelengths larger than X_b, the growth rate matches that of the instability predicted by the one-line approximation for an angle at breaking which is above the angle maximizing alongshore transport.

Key words: shoreline sand waves, high-angle waves, surf zone rhythmic bars, alongshore sediment transport, one-line shoreline modelling

1. Introduction

The shorelines of sandy coasts are hardly straight but quite often display undulations at various lengthscales. These undulations are sometimes relatively regular or even nearly alongshore periodic with a wavelength λ, suggesting that they are the imprint of a physical mechanism dominating the dynamics of this stretch of coast with λ being its characteristic length scale. Perhaps the most known are *beach cusps* that may develop at the swash zone and typically have horn-to-horn distances of $\lambda \sim$ 1-50 m (Almar et al., 2008). At a larger scale, shorelines may display undulations with a wavelength in the range $\lambda \sim$ 100-1000 m that are known as *megacusps*. They are linked to crescentic bars, to transverse bars or, more generally, to rip channel systems (Orzech et al., 2011). In case of transverse bars, their apexes develop at the shore attachements of the bars and the embayments in between correspond to the troughs in between bars. Megacups can also form due to the influence of a crescentic bar on the circulation and the waves shoreward of it (Ribas et al., 2015). Finally, shorelines may display undulations at a scale which is even larger than surf zone rhythmic bars, i.e., $\lambda >> X_b$, where X_b is the width of the surf zone. These large scale undulations have typical alongshore wavelengths > 1 km (on open ocean beaches) and are linked to similar undulations in the depth contours well offshore the surf zone. They have been called *km-scale shoreline sand waves* (Idier and Falqués, 2014).

Shoreline features may be forced by external templates in the hydrodynamics (waves and currents) or by the antecedent geological constraints. However, they can also be self-organized, that is, they can emerge out of the internal dynamics of the coastal system (Coco and Murray, 2007). In this case the wavelength λ and the particular pattern both in the morphology and the hydrodynamics are not dictated by the external forcing but by the internal dynamics. The common approach to understand the emergence of self-organized patterns is as follows. A basic steady equilibrium state without the pattern is assumed. Then an arbitrary perturbation of the morphology is introduced. This causes an alteration of the hydrodynamics, hence of sediment transport. The gradients in sediment transport create areas of deposition and areas of erosion. If the bathymetric changes reinforce the initial perturbation a positive feedback occurs and the perturbation both in the morphology and in the hydrodynamics will grow. The initial perturbation can in fact be either in the morphology or in the hydrodynamics or in both. This can be studied mathematically by doing the

[1]Physics Department, UPC, Barcelona, Catalonia, Spain. albert.falques@upc.edu

stability analysis of the basic equilibrium state and the emerging patterns are the instability modes. This approach allows understanding the formation of beach cusps (Coco et al., 2000, Dodd et al., 2008), crescentic bars (Deigaard, 1999, Falqués et al., 2000, Calvete et al., 2005) and transverse bars (Ribas et al., 2003, Garnier et al., 2006, Ribas et al., 2012).

The dynamics of wave-dominated sandy shorelines at large length scales $>>X_b$ can be described with the one-line approximation (see, e.g., Komar, 1998) in which the surf zone collapses in one line (the shoreline). The changes in shoreline position are then governed by the alongshore gradients in the total alongshore sediment transport rate, Q (total volume per time unit). In this context and as it is shown in Figure 1, a cuspate foreland will cause gradients in Q and it will grow if Q decreases moving from the updrift side (A) to the downdrift side of the apex (B). The sediment transport rate is commonly computed with semi-empirical formulae (e.g., the CERC formula) and depends on the wave height H_b and on the angle between wave fronts and local shoreline at breaking, α_b:

$$Q = Q(H_b, \alpha_b) \tag{1}$$

The Q function increases with H_b but regarding the angle it is increasing up to a critical angle $\alpha_{bc} \sim 45^o$ and it is decreasing for $\alpha_b > \alpha_{bc}$. Then, assume first that the shoreline undulation do not affect the bathymetric contours that keep on being rectilinear and parallel to the undisturbed shoreline. In this case, H_b does not change along the shore. Let us also assume $\alpha_b > \alpha_{bc}$, i.e., Q is decreasing by increasing α_b. Since the wave angle (relative to the local shoreline) increases moving from updrift of the apex (A) to downdrift of it (B), Q will decrease so that the cuspate foreland will grow (situation shown in Figure 1). On the contrary, if the angle is below the critical value, $\alpha_b < \alpha_{bc}$, the cuspate foreland will decay. This is a first type of instability, which will be referred to as EHAWI (the motivation for this term is explained later on). Although it was first proposed a long time ago by Zenkovitch (1959) it has been largely ignored because, due to bathymetric refraction, the wave angle at breaking hardly reaches the critical one, $\alpha_{bc} \approx 45^o$. However, the depth contours tend to deform following the undulation of the shoreline. As a result there are differences in refractive wave crest stretching between updrift (A) and downdrift (B) so that H_b tends to be larger updrift than downdrift. This makes Q to be larger at (A) so that it favors instability that would then occur for angles $\alpha_b < \alpha_{bc}$. Studying this second option requires defining a link between the shoreline undulations and the bathymetric undulations and it is found that shoreline instability occurs for $\alpha_0 > \alpha_{0c}$, where α_0 is the wave angle at the depth of closure, D_c, that is, the maximum depth where the shoreline undulation can be noticed in the depth contours. It turns out that $\alpha_{0c} \sim \alpha_{bc}$. This second type of instability is more plausible as wave angles at D_c can be much larger than at breaking. We call it HAWI (High-angle wave instability) after Ashton et al. (2001) and it has been extensively studied in recent years (Ashton et al., 2001, Falqués and Calvete, 2005, Ashton and Murray, 2006, Medellin et al, 2009, Ashton et al., 2009, van den Berg et al., 2012, Kaergaard and Fredsoe, 2013, Idier and Falqués, 2014). The aim of the present contribution is investigating EHAWI (Extreme high-angle wave instability), that is, the instability associated to a large wave angle *at breaking*. The essential difference between both instabilities is that HAWI is associated to a link between the surf and shoaling zones while EHAWI is just related to the surf zone. We will explore the instability both in the one-line and in the 2DH approaches. We will show that in some particular situations, the wave angle at breaking can indeed be large enough to trigger such instability and we will explore the emerging patterns and their characteristic wavelength.

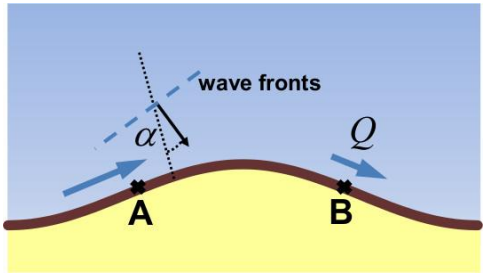

Figure 1. Alongshore distribution of total sediment transport rate leading to the growth of a sandy cuspate foreland and definition of the wave angle relative to local shoreline orientation, α.

2. One-line approach

Let us assume a Cartesian coordinate system with y along the unperturbed shoreline, x normal to it pointing seawards and z vertical upwards. According to sediment conservation, the governing equation for the perturbed shoreline, $x_s(y,t)$, is (Komar, 1998)

$$\frac{\partial x_s}{\partial t} = -\frac{1}{D_c}\frac{\partial Q}{\partial y} \tag{2}$$

Then, if ϕ is the (small) angle of the local shoreline orientation with respect to the y axis, $\partial x_s/\partial y = \tan\phi \approx \phi$, we have

$$\frac{\partial Q}{\partial y} = \frac{\partial Q}{\partial \phi}\frac{\partial \phi}{\partial y} = -\frac{\partial Q}{\partial \theta}\frac{\partial \phi}{\partial y}$$

since $\alpha = \theta - \phi$, where θ is the absolute wave angle with respect to the unperturbed shoreline. Therefore, a diffusion equation follows as governing equation (Pelnard-Considère, 1956):

$$\frac{\partial x_s}{\partial t} = \varepsilon \frac{\partial^2 x_s}{\partial y^2} \tag{3}$$

with

$$\varepsilon = \frac{1}{D_c}\frac{\partial Q}{\partial \theta} \quad .$$

For $\theta_b > \theta_{bc}$, $\partial Q/\partial\theta < 0$, and the diffusivity is negative. In this case, the shoreline is unstable and there is no wavelength selection, since the smaller is the shoreline undulation wavelength, the larger is its growthrate. This is easily seen by inserting a shoreline perturbation of the form:

$$x_s(y,t) = Ae^{\sigma t + iKy} + c.c.$$

in Equation (3), where c.c. means complex conjugate, A is a constant small amplitude, σ is the complex growthrate and $\lambda = 2\pi/K$ is the wavelength. Then,

$$\sigma = -\varepsilon K^2 \tag{4}$$

is obtained (see Figure 4).

In case of using the CERC formula (Komar, 1998):

$$Q = \mu H_b^{5/2}\sin(2\alpha_b)$$

$\theta_{bc} = 45^o$ and the diffusivity,

$$\varepsilon = \frac{2\mu}{D_c}\cos(2\alpha_b) \tag{5}$$

is clearly negative for $\theta_{bc} > 45^o$.

In nature, however, the one-line approximation does not make sense for length scales ~ X_b or smaller. Therefore, this simple computation suggests that the shoreline will be unstable in case $\theta_b > \theta_{bc}$ but there is no way to find out the characteristic wavelength of such instability. Moreover, the one-line approximation is a very crude representation of reality; it remains unknown whether the instability will survive if the surf-zone processes are included in the modelling.

3. 2DH stability model

We use the morfo60 linear stability model describing the coupling between waves, depth-averaged currents and bathymetric changes in the surf zone with 2 horizontal dimensions. The model is described in more detail in Calvete et al. (2005) and Ribas et al. (2012) and here we only revisit the main features. The

coordinate system defined in section 2 is used but, as needed, (x_1, x_2) will stand for (x,y). The shoreline is formally fixed (y=x_2=0) in this model, but a shoal (deep) developing near the shoreline can be physically interpreted as a shoreline progradation (retreat).

3.1 Waves

Waves are assumed to have a narrow spectrum in frequency and angle. Their heights are supposed to follow the Rayleigh distribution, characterized by the root mean square wave height, H_{rms} (wave energy being $E = \rho g H_{rms}^2/8$, where ρ is the water density and g is gravity). When they approach the coast, their transformation is described using linear wave theory, which yields expressions for the wave properties such as the radiation stresses, S^w_{ij}, the root mean square wave orbital velocity amplitude, u_{rms}, and the two components of the group and phase velocity, c_{gi} and c_i. The dispersion relation reads

$$\omega = \sqrt{g|\nabla\Phi|\tanh\left(|\nabla\Phi|D\right)} + v_j \frac{\partial\Phi}{\partial x_j} \quad , \tag{6}$$

where ω is the absolute frequency and the Doppler shift is accounted for. In this equation and hereinafter, dummy indices are assumed to be summed, e.g., over j=1,2. Here, Φ, is the phase, from where the wavenumber and the wave angle are computed through $k_i = \partial\,\Phi / \partial\, x_i$. The two components of the depth-averaged fluid velocity are v_i, $D = z_s - z_b$ is the water depth, where z_s is the mean free surface level, and z_b is the sea bed level. Steady conditions are assumed, ω = constant. This equation describes the refraction and shoaling of the waves due to both topography and currents. More complex processes in wave propagation, like wave diffraction, are not accounted for.

Wave energy balance is described with a wave- and depth-averaged equation (with wave-current interactions),

$$\frac{\partial E}{\partial t} + \frac{\partial}{\partial x_j}\left(\left(v_j + c_{g\,j}\right)E\right) + S^w_{jk}\frac{\partial v_k}{\partial x_j} = -\mathcal{D}_w \tag{7}$$

where the wave energy dissipation $\mathcal{D}_w$ is computed with the Church and Thornton (1993) formulation. The energy dissipated by breaking feeds the surface rollers, i.e. the aerated mass of water located on the shoreward face of breaking waves. The wave- and depth-averaged roller energy balance is

$$\frac{\partial\left(2E_r\right)}{\partial t} + \frac{\partial}{\partial x_j}\left(2\left(v_j + c_j\right)E_r\right) + S^r_{jk}\frac{\partial v_k}{\partial x_j} = -\mathcal{D}_r + \mathcal{D}_w \tag{8}$$

where E_r is the energy of the roller, S^r_{ij} are the radiation stresses due to roller propagation and $\mathcal{D}_r$ is the roller energy dissipation rate. Given ω=2π/T_p, H_{rms} and θ at the offshore boundary, equations (4), (5) and (6) allow computing k, θ and H_{rms} in the whole domain.

3.2 Mean hydrodynamics

The mean fluid motions are governed by the wave- and depth-averaged mass and momentum balance equations, where the radiation stresses due to both wave and roller propagation are included,

$$\frac{\partial D}{\partial t} + \frac{\partial}{\partial x_j}\left(D v_j\right) = 0 \tag{9}$$

$$\frac{\partial v_i}{\partial t} + v_j\frac{\partial v_i}{\partial x_j} = -g\frac{\partial z_s}{\partial x_i} - \frac{1}{\rho D}\frac{\partial}{\partial x_j}\left(S^w_{ij} + S^r_{ij} - S^t_{ij}\right) - \frac{\tau_{bi}}{\rho D} \quad , \qquad i = 1,2 \quad , \tag{10}$$

and where, τ_{bi} are the bed shear stresses and S^t_{ij} are the turbulent Reynolds stresses. They are modelled with the standard eddy viscosity approach. The lateral turbulent mixing coefficient is directly linked to the roller energy dissipation, $\mathcal{D}_r$, (the main source of turbulence), $\upsilon_t = M\,(\mathcal{D}_r/\rho)^{1/3}$, where $M = 1$. The fluid

velocities are imposed to be zero at both the coastline and the offshore boundary. Also, the free surface elevation is zero at the offshore boundary.

3.3 Sediment transport and bed updating

Conservation of sediment mass yields the bottom evolution equation

$$(1-p)\frac{\partial z_b}{\partial t}+\frac{\partial q_j}{\partial x_j}=0 \quad . \tag{11}$$

with $p=0.4$ being the porosity of the bed and q_i the two components of the wave- and depth-averaged volumetric sediment transport (m^2/s). A widely accepted formulation for q_i in the nearshore is that of Soulsby and van Rijn (Soulsby, 1997). Their original expression has been extended to model the effect of a 2-dimensional flow and the preferred downslope transport of the sand,

$$q_i = C\left(v_i - \Gamma\frac{\partial h}{\partial x_i}\right) \quad , \qquad i=1,2 \quad , \tag{12}$$

where C is the depth-integrated volumetric sediment concentration. The bed slope term, proportional to Γ, accounts for the tendency of the system to smooth out the sea bed perturbations, h, if the latter do not cause a positive feedback into the flow. The sediment concentration, C, is a function of the current, the wave orbital velocity and the roller energy dissipation. However, since we want to seek the instability suggested by the one-line modelling, we will assume C=const. to avoid introducing specific features of 2DH formulations that would not be represented in the one-line approximation.

3.4 Linear stability analysis

The equations (5), (6), (7), (8), (9) and (10), which govern this morphodynamic system, together with the parameterizations used and the appropriate boundary conditions, define a closed dynamical system for the variables v_1, v_2, z_s, E, E_r, Φ and z_b. The stability analysis starts by defining a steady and alongshore uniform basic state (i.e., without the alongshore rhythmic patterns), which is defined by an equilibrium beach profile, $z_b = z^o_b(x)$, and the wave parameters at the offshore boundary, H_{rms}, T_p and θ at the offshore boundary. The modeled basic state is characterized by the presence of a longshore current, $v^o_1 = 0$ and $v^o_2 = V^o(x)$, and an elevation of the mean sea level, $z^o_s = z^o_s(x)$. This basic state represents a morphodynamic equilibrium only under the assumption that the net cross-shore sediment flux is zero. Once the variables in the basic state are computed, a perturbed state of the form

$$(v_1, v_2, z_s, E, E_r, \Phi, z_b) = (0, V^o, z^o_s, E^o, E^o_r, \Phi^o, z^o_b) + e^{(\sigma t + iK y)}(u, v, \eta, e, e_r, \phi, h) \quad + c.c. \tag{13}$$

is assumed, where the superscript ^{o} stands for the basic state variables. By inserting equation (11) into the governing equations and linearizing with respect to the perturbations, an eigenproblem is obtained where σ is the eigenvalue and ($u(x)$, $v(x)$, $\eta(x)$, $e(x)$, $e_r(x)$, $\phi(x)$, $h(x)$) are the eigenfunctions. For each perturbation wave number, $K=2\pi/\lambda$, a number of eigenvalues σ with the corresponding eigenfunctions exist, which characterize the different growing (or decaying) modes. The growth rate of the emerging features is given by $\sigma_r = \mathcal{Re}(\sigma)$, so that $\sigma_r > 0$ means growth. In case of an unstable basic state, solutions with $\sigma_r > 0$ are found and the instability curves show these positive σ_r for different values of K. Starting from arbitrary small initial perturbations, the dynamics after some time will be dominated by the mode with largest growth rate, which is called Fastest Growing Mode (FGM). Its characteristic growth time (e-folding growth time) is given by σ_r^{-1} and the alongshore migration speed by $c = -\mathcal{Im}(\sigma)/K$. The possible emerging patterns in the wave field, the mean hydrodynamics and the morphology are defined by the eigenfunctions corresponding to the growing modes.

4. 2DH stability computations

4.1 Basic state

For the sake of simplicity and keeping as close as possible to the one-line approach, we use a planar reference beach profile, $z^o_b(x) = -\beta x$, with $\beta = 0.02$. We assume H_{rms} = 1 m and T_p=6 s at D_{off} = 20.3 m. Wave angles at D_{off} are explored from $\theta_{off} = 0$ to $\theta_{off} = 90^o$. The depth integrated sediment concentration is C=0.002 m. Regarding the bed slope coefficient, the values Γ= 0.1, 0.01, 0.001 and 0 m/s will be explored. The characteristics of the basic state for $\theta_{off} = 70^o$ are shown in Figure 2. The surf zone width is $X_b \approx 110$ m, the maximum current is $V_m \approx 0.7$ m/s at $x \approx 40$ m and the wave angle at breaking is $\theta_b \approx 28^o$.

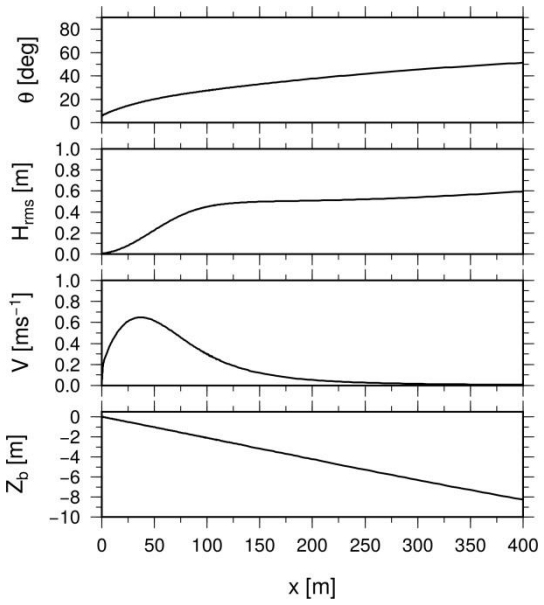

Figure 2. Basic state for the instability analysis, for T_p=6 s, $\theta_{off} = 70^o$ and $H^{off}_{rms} = 1$ m.

4.2 Instability mode for high-angle waves

Wavelengths in the range λ =0-1000 m are explored. To keep our 2DH analysis close to the one-line approach the bed-slope transport should be switched off by taking $\Gamma = 0$. In this case however many spurious unstable modes appear (purely numerical eigenvalues, see, e.g., Calvete et al., 2005) and

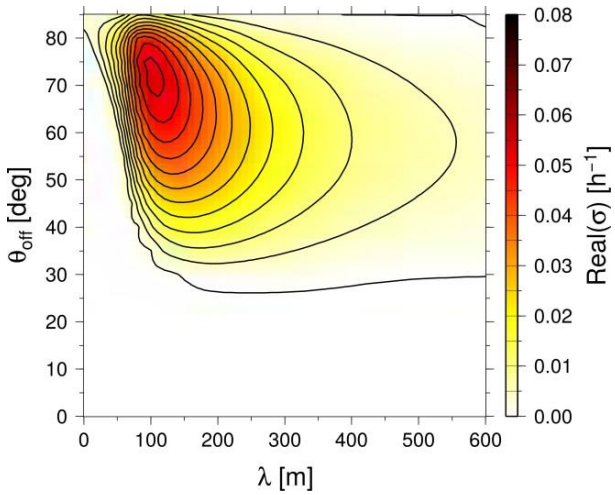

Figure 3. Contour lines of instability growth rate as a function of the alongshore wavelength, λ, and the offshore wave angle, θ_{off}.

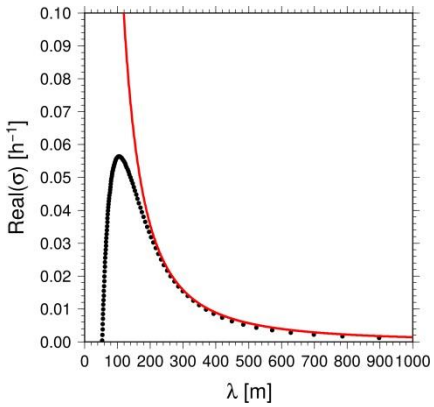

Figure 4. Instability curves for: EHAWI with the one-line approximation (Equation 4) for $\varepsilon = -0.01$ m^{2}s^{-1} (red thick line) and for the 2DH instability mode with θ_{off}=70^o (black dotted line).

physically reliable solutions cannot be identified. On the contrary, for Γ = 0.1, 0.01, 0.001 m/s only one growing instability mode is found in the λ =0-1000 m range. This mode is qualitatively very similar for the different Γ values and it seems that it converges in the limit $\Gamma \to 0$. Here we discuss the results of the Γ = 0.01 m/s case, which are therefore representative of such limit.

Interestingly and as it is shown in Figure 3, the instability develops only for $\theta_{off} > 30^o$. Its maximum intensity occurs for $\theta_{off} \approx 70^o$ with a characteristic growth time $\sigma_r^{-1} \approx 18$ h and a wavelength $\lambda \approx 105$ m. The downdrift migration celerity is c $\approx$ 8 m/h. The growing mode for $\theta_{off} = 70^o$ is shown in Figure 4. It is seen that this mode grows only for $\lambda > 50$ m, the maximum growth occurs for $\lambda \approx 105$ m and for $\lambda \approx 1000$ m the growth rate becomes negligible. The perturbed depth contours (Figure 5) correspond to wide oblique bars that are upcurrent-oriented, that is, the distal tip of the bars are shifted updrift with respect to the shore-attachment (Ribas et al., 2015). Although the model does not describe it explicitly, at the shore attachment of the bars a megacusp would develop in reality and shoreline embayments would occur where the troughs meet the shoreline. Coupled to the growing morphology there is a meandering in the longshore current so that the current veers seaward updrift of the bars and shoreward downdrift of the bars. The maximum current intensity occurs at the lee of the bars. At large wavelengths this mode also grows but much more slowly. For example, for λ=900 m the characteristic growth time is 36 d. As shown in Figure 6, in this case it displays long bathymetric undulations and the bars are hardly visible.

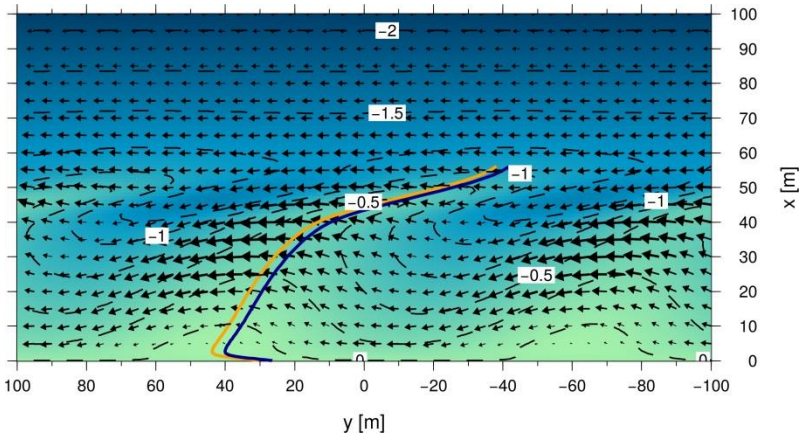

Figure 5. Perturbed bathymetry and perturbed longshore current for the dominant wavelength, λ=105 m (2 wavelengths are shown). An arbitrary amplitude for the perturbation has been chosen to ease visualization. The shore is at the bottom of the plot and the wave incidence is from the left. Deep blue color represents deeper areas while lighter colors represent shallower areas. The yellow line indicates the crest of a bar, $y=F(x,y_0)$. The blue line is the line parallel to the bar crest with maximum total sediment transport rate across it, $Q^*(y)$.

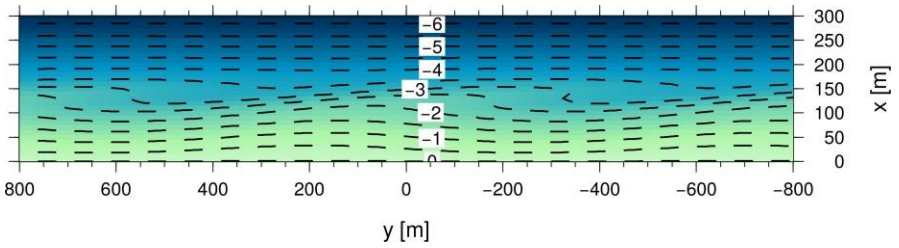

Figure 6. Bathymetric pattern of the instability mode for θ_{off}=70º for a large wavelength, λ=900 m. An arbitrary amplitude for the perturbation has been chosen. The shore is at the bottom of the plot and the wave incidence is from the left. Deep blue color represents deeper areas while lighter colors represent shallower areas.

The growth rate corresponding to EHAWI for the one-line modelling, $\sigma = -\varepsilon\,(2\pi/\lambda)^2$ (Equation 4) is also plotted in Figure 4. It is remarkable that by selecting a suitable value of the diffusivity, $\varepsilon = -0.01$ m^{2}s^{-1} in this case, the long wavelength tale of the 2DH instability curve fits very well the EHAWI instability curve. This gives confidence in the 2DH instability mode as being the 2DH counterpart of EHAWI. By representing the alongshore transport with the CERC formula, with H_b = 1 m and a common value μ=0.2 m$^{1/2}$s^{-1}, and by assuming D_c=5 m, the $\varepsilon = -0.01$ m^{2}s^{-1} diffusivity (Equation 5) is obtained for $\theta_b \approx 47^o$.

4.3 Analysis of the longshore sediment transport

To relate the 2DH instability mode with the EHAWI instability coming out of the one-line approach we try to define a magnitude playing the role of the total alongshore transport rate Q but in the 2DH approach. The straightforward option would be the integral of the alongshore sediment flux in any cross-section from the shoreline, x=0, to the offshore boundary, x=x_{off}. But since the bathymetric undulations are shifted with respect to the associated shoreline undulation (upcurrent-oriented bars), the alongshore gradients in this magnitude could not be easily linked to the growth/decay of the morphological features contrarily to what happens for Q in the one-line approach. Therefore, consider for each x_0 the crest of a bar as the position of the maximum bed level following alongshore the line x=x_0. Then, if y=$f(x)$ is the crest of the bar that attaches at the shoreline at y=0, we define the line which is parallel to that bar crest and meets the shoreline at y=y_0 by (see Figure 7):

$$y = F(x, y_0) = y_0 + f(x)$$

Finally, we define the total sediment transport rate crossing the lines that are parallel to the crests by:

$$Q^*(y_0) = \int_0^{s_{off}} \vec{q} \cdot \hat{n}\, ds \tag{12}$$

where the integral is done along the line y=$F(x,y_0)$, $\hat{n}$ is the unit normal vector to this line pointing downdrift, and s is the length along this line. Thereinafter we will refer to Q^* as the *total cross-bar sediment transport rate*. Let us consider the region $\boldsymbol{S}$ bounded by two of these lines, y=$F(x,y_1)$, y=$F(x,y_2)$, by the shoreline, x=0, and by the offshore boundary, x=x_{off}. Let y=$F(x,y_1)$ and y=$F(x,y_2)$, with $y_1 < y_2$, be its updrift and downdrift boundaries, respectively. Then, since there is sediment flux only across these two lateral boundaries, if $Q^*(y_1) > Q^*(y_2)$, there will be convergence of sediment in $\boldsymbol{S}$ so that the mean sea bed in $\boldsymbol{S}$ will rise on average. Therefore, as in the one-line approach, the morphological feature will grow if Q^* decreases moving from updrift to downdrift of the shoreline apex or, in other words, if the maximum in $Q^*(y)$ is shifted updrift with respect to the apex (between the apex and the updrift embayment). Figure 8 shows that, indeed, this is the case for the 2DH instability mode and it can therefore be associated to the one-line instability based on the gradients in Q.

5. Discussion

The surf zone morphodynamic instability mode we have found shares the essential characteristics of the

EHAWI in the famework of the one-line shoreline dynamics approximation:

1. It occurs only above a critical angle $\theta_{off} \sim 30^o$ and it has its maximum growth for very high angle waves with $\theta_{off} \sim 70^o$.
2. For relatively large wavelengths, the growth rate follows an anti-diffusional behavior that is fully consistent with the one-line approach.
3. It is related to the alongshore gradients in total alongshore sediment transport rate (Q^*).
4. It does not depend essentially of the coupling between the surf and shoaling zones through cross-shore sediment transport and it develops only in the surf zone.

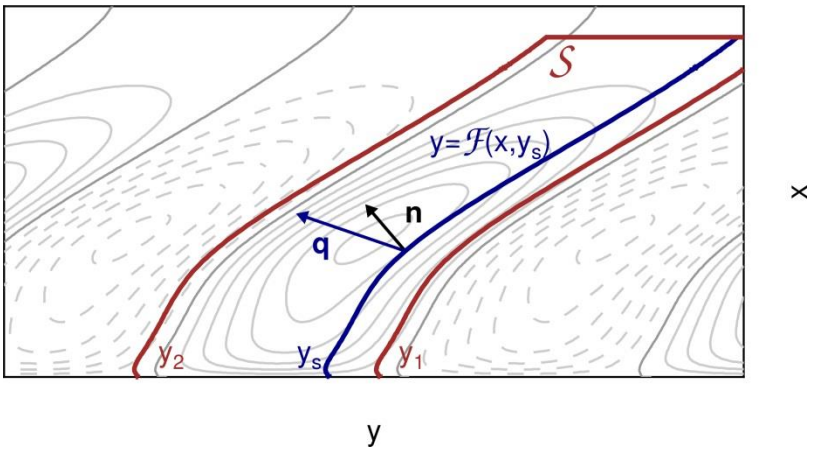

Figure 7. Control volume ***S*** to analyze the growth or decay of morphological features as a function of the total along-current sediment transport rate, Q^*. Downdrift direction is from right to left. The contour lines of the bed level perturbation are also shown (solid lines correspond to bars, dashed lines correspond to troughs).

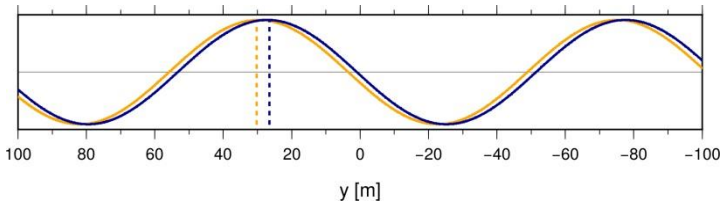

Figure 8. Alongshore distribution of the alongshore sediment flux (blue line) in comparison with the shoreline undulation (yellow line). Downdrift direction is from right to left.

However, EHAWI develops for wave angles at breaking larger than that maximizing the sediment transport rate, $\theta_b > \theta_{bc} \sim 45^o$ while the 2DH instability occurs for lower angles at breaking, $\theta_b \sim 30^o$. It might happen that the maximum alongshore transport in case of resolving the surf zone occurs for angles smaller than 45^o. In fact, it is very striking that the maximum intensity of the instability occurs for an offshore angle $\theta_{off} \approx 62^o$, which is the offshore angle that maximizes the angle at breaking (see Figure 9). This clearly suggests that the instability is associated to a large wave angle at breaking.

On the other hand, surf zone morphodynamic instabilities leading to up-current oriented oblique bars had already been studied (e.g., Ribas et al., 2003, Ribas et al., 2012) and the results are quite similar to those for the present 2DH surf zone instability mode. Importantly, the bars develop only for quite oblique wave incidence. The gradients in the alongshore transport had not explicitly been examined in the analysis of the formation mechanism but since there is a seaward directed cross-shore component of the meandering current on the bars, mass conservation implies convergence of the longshore component on the bars. The new aspect of the present study is the connection with EHAWI in the framework of the one-line approximation. The conclusion would be that there could be a number of different self-organized surf zone rhythmic patterns associated to high-angle waves. The morphology and the specific formation mechanism depend on the basic bathymetric profile and wave conditions and, in particular, on the depth averaged

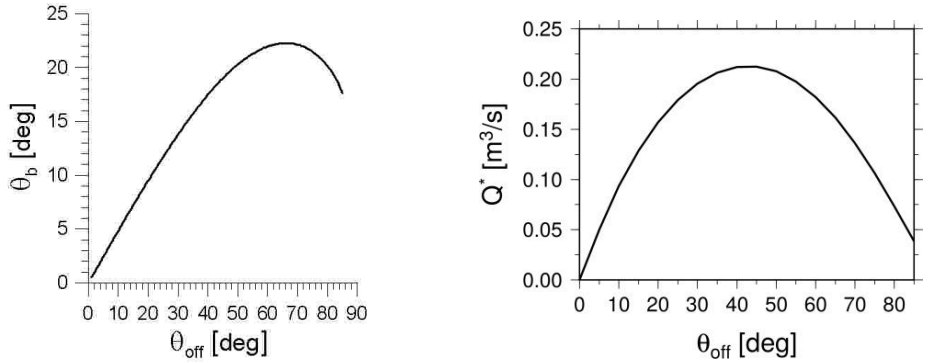

Figure 9. Wave angle at breaking (left panel) and total cross-bar sediment transport rate, Q^* , for the basic state (right panel), as a function of the angle in deep water (D_{off}=20.3 m) for T_p=6 s, H_{rms}^{off} =1 m, γ_b=0.5.

sediment concentration (Ribas et al., 2015). But all of them are essentially associated to large wave incidence angles and they can be considered as the counterpart of EHAWI in surf zone morphodynamics.

6. Conclusions

One-line shoreline modelling shows that self-organized shoreline sand waves without associated bathymetric undulations in the shoaling zone can emerge if the wave angle at breaking is higher than about 45^o (EHAWI: extreme high-angle wave instability). In the framework of the one-line modelling this instability does not have a preferred wavelength and it was not clear how it behaves when 2DH surf zone morphodynamics is resolved. We have investigated it with a linear stability model describing surf zone morphodynamic instabilities. A single unstable mode growing only for high-angle waves, above a critical angle of about 30^o, is found. Its maximum growth rate occurs for about 70^o with a characteristic growth time of about 20 h. It consists of oblique up-current oriented bars with a dominant wavelength of the order of the surf zone width. Its growth is coupled to a meandering in the longshore current and is related to the gradients in alongshore sediment transport. It weakly depends on the diffusive downslope sediment transport and it converges for this transport tending to 0. It can also form with large wavelengths, e.g., $\lambda \approx$ 900 m, with a characteristic growth time of 36 d. For relatively large wavelengths the growth rate matches very well the anti-diffusional behavior of EHAWI that is found with one-line modelling. It seems therefore that this mode could be the 2DH counterpart of the EHAWI. However, other surf zone rhythmic patterns related to high-angle waves that had already been studied (see, e.g., Ribas et al., 2012) could also play this role. More research should be conducted in the future to compare the different physical mechanisms behind each pattern and its relation with the simple one-line instability. Furthermore, the investigation of the instability mode presented here is very preliminary and its sensitivity to the basic profile, to the wave conditions and to the sediment transport formulation should be examined.

Acknowledgements

This research is part of the project CTM2015-66225-C2-1-P funded by the Spanish Government and cofunded by the E.U. (FEDER).

References

Almar, R., Coco, G., Bryan, K.R., Huntley, D.A., Short, A.D. and Senechal, N., 2008. Video observations of beach cusp morphodynamics, *Mar. Geology*, 254: 216-223.

Ashton, A., Murray, A. B. and Arnault, O., 2001. Formation of coastline features by large-scale instabilities induced by high-angle waves, *Nature*, 414: 296-300.

Ashton, A. and Murray, A.B., 2006. High-angle wave instability and emergent shoreline shapes: 1. Modeling of sand waves, flying spits, and capes. *J.Geophys.Res.*, 111, F04011,doi:10.1029/2005JF000422.

Ashton, A.., Murray, A.B., Littlewood, R., Lewis, D.A. and Hong, P, 2009. Fetch-limited self-organization of elongate water bodies. *Geology*, 37:187-190.

Coco, G., Huntley, D.A. and O'Hare, T.J., 2000. Investigation of a self-organization model for beach cusp formation and development. *J. Geophys. Res.*, 105(C9): 21991-22002.

Coco, G. and Murray, A.B., 2007. Patterns in the sand: From forcing templates to self-organization. *Geomorphology*, 91:271-290.

Dodd, N., Stoker, A., Calvete, D. and Sriariyawat, A., 2008. On Beach Cusp Formation. *J. Fluid Mech.*, 597:145-169.

Falqués, A. and Calvete, D., 2005. Large scale dynamics of sandy coastlines. Diffusivity and instability. *J. Geophys. Res.*, 110(C03007), doi:10.1029/2004JC002587.

Garnier, R., Calvete, D., Falqués, A. and Caballeria, M., 2006. Generation and nonlinear evolution of shore-oblique/transverse sand bars. *J. Fluid Mech.*, 567:327-360.

Idier, D. and Falqués, A., 2014. How kilometric sandy shoreline undulations correlate with wave and morphology characteristics: preliminary analysis on the Atlantic coast of Africa. *Adv. Geosciences*, 39:55-60.

Kaergaard, K. and Fredsoe, J., 2013. Numerical modeling of shoreline undulations part 1: Constant wave climate. *Coastal Eng.*, 75:64-76.

Komar, P.D., 1998. *Beach Processes and Sedimentation*. Prentice Hall.

Medellín. G., Falqués, A., Medina, R. and González, M., 2009. Sand waves on a low-energy beach at 'El Puntal' spit, Spain: Linear Stability Analysis. *J. Geophys. Res.* 114(C03022), doi:10.1029/2007JC004426.

Orzech, M.D., Reniers, A.J.H.M., Thornton, E.B. and MacMahan, J.H., 2011. Megacusps on rip channel bathymetry: Observations and modeling. *Coast. Eng.*, 58:890-907.

Ribas, F., Falqués, A. and Montoto, A., 2003. Nearshore oblique sand bars. *J. Geophys. Res.*, 108(C43119), doi:10.1029/2001JC000985.

Ribas, F., de Swart, H.E., Calvete, D. and Falqués, A., 2012. Modeling and analyzing observed transverse sand bars in the surf zone. *J. Geophys. Res.*, 117 (F02013), doi:10.1029/2011JF002158.

Ribas, F., Falqués, A., de Swart, H.E., Dodd, N., Garnier, R. and Calvete, D., 2015. Understanding coastal morphodynamic patterns from depth-averaged sediment concentration. *Rev. Geophys.*, 53, doi:10.1002/2014RG000457.

Van den Berg., N., Falqués, A. and ribas, F., 2012. Modelling large scale shoreline sand waves under oblique wave incidence. *J. Geophys. Res.*, 117(F03019), doi:10.1029/2011JF002177.

Zenkovitch, V.P., 1959. On the genesis of cuspate spits along lagoon shores. *J. Geology*, 67:269-277.